International Journal of Mass Spectrometry 302 (2011) 139–148

Contents lists available at ScienceDirect

International Journal of Mass Spectrometry

journal homepage: www.elsevier.com/locate/ijms

Structural characterization of both the non-proteolytic and proteolytic activation pathways of coagulation Factor XIII studied by hydrogen–deuterium exchange mass spectrometry

Mette Dahl Andersen*, Johan Henrik Faber

Department of Protein Structure and Biophysics, Biopharmaceutical Research Unit, Novo Nordisk A/S, Novo Nordisk Park, DK-2760 Måløv, Denmark

ARTICLE INFO

Article history:
Received 28 May 2010
Received in revised form 31 August 2010
Accepted 9 September 2010
Available online 17 September 2010

Keywords:
Factor XIII
Hydrogen–deuterium exchange
Enzyme activation
Structure–activity relationship
Transglutaminases
rFXIII

ABSTRACT

Activated Factor XIII is a 83 kDa transglutaminase crucial in the final steps of blood coagulation. FXIII can be activated both via a proteolytic pathway and a non-proteolytic pathway. Activation in plasma takes place by a thrombin catalyzed cleavage after residue Arg37 (FXIIIa′) and a Ca^{2+} dependent conformational change (FXIIIa*). The non-proteolytic activation is the result of a conformation change only in the absence of thrombin or other proteolytic cleavage (FXIIIa◦). Hydrogen/deuterium exchange (HX) detected by mass spectrometry (MS) has proven a powerful technique for analyzing the conformational properties of proteins in solution. In this study, we apply HX-MS analyses on the entire span of conformational states of recombinant FXIII, i.e., rFXIII, rFXIIIa′, rFXIIIa* and rFXIIIa◦. 79 peptic peptides were used for analysis providing 90% coverage of the 83 kDa non-redundant sequence of FXIII. The HX-MS data show increased deuterium exchange along the dimer interface suggesting weakened dimer interaction in all rFXIIIa′, rFXIIIa* and rFXIIIa◦. Apart from this, rFXIIIa′ resembles zymogen rFXIII and no conformational changes seem to have taken place. In contrast, extensive changes occur upon full activation to either rFXIIIa* or rFXIIIa◦. All domains of rFXIII are involved, but the major changes occur in the catalytic core and β-barrel 1 domains. Furthermore, these experiments show highly similar HX-MS data for rFXIIIa* and rFXIIIa◦ clearly demonstrating that both the thrombin dependent and the non-proteolytic activation pathways of rFXIII produce similar activated conformations.

1. Introduction

Activated Factor XIII (FXIII; EC 2.3.2.13) is a transglutaminase catalyzing intermolecular ε-(γ-glutamyl)lysine isopeptide bonds [1]. FXIII activity is crucial in the final steps of blood coagulation by cross-linking fibrin monomers into a tight fibrin network. Furthermore, a number of anti-fibrinolytic, pro-haemostatic and adhesive proteins are cross-linked to the clot thereby providing a mechanically strong fibrin structure with increased resistance to fibrinolysis by plasmin or other proteolytic enzymes. FXIII is also found intracellular where the cross-linking enzyme activities are involved in tissue remodeling and also in cytoskeleton remodeling that occurs, for instance, during platelet activation [2–4]. (See [5–9] for reviews on FXIII structure and function.)

The catalytic activity is located in the 83 kDa FXIII – A subunit which forms a stable non-covalent dimer structure in solution. The dimer structure of rFXIII has been characterized various times by X-ray crystallography (Fig. 1A) [10–12]. Each FXIII–A subunit consists of an N-terminal activation peptide (residues 1–37), a β-sandwich domain, the large catalytic core domain holding the active site residues Cys314, His373 and Asp396 and finally two β-barrel domains (Fig. 1A and D). The dimer structure of rFXIII shows the activation peptide of one rFXIII subunit extending towards the catalytic core domain of the opposite rFXIII subunit and thus close to the opposite active site (Fig. 1A). Plasma FXIII furthermore contains two 80 kDa non-catalytic carrier FXIII-B subunits and thus circulates as a hetero-tetramer. Intracellular FXIII consists of the FXIII-A subunits only.

In plasma, thrombin hydrolyzes the activation peptide of FXIII between residues Arg37-Gly38 resulting in FXIIIa′ (Fig. 2B). This event does not by itself create functional enzyme activity, e.g., the active site Cys314 is not solvent exposed in FXIIIa′ [13,14] and thrombin cleaved FXIIIa′ retains a zymogen conformation [15]. In the presence of physiological plasma concentrations of Ca^{2+} and

Abbreviations: ESI, electrospray ionization; MALDI, matrix assisted laser desorption/ionization; MS, mass spectrometry; HX, hydrogen/deuterium exchange; HEPES, 4-(2-hydroxyethyl)piperazine-1-ethanesulfonic acid; CID, collision induced dissociation; UPLC, ultra performance liquid chromatography; FXIII, Factor XIII; rFXIII, recombinant FXIII (consisting of the A_2 subunits); FXIIIa*, thrombin activated FXIII; FXIIIa′, thrombin cleaved but not active; FXIIIa◦, FXIII activated without proteolysis; TG, transglutaminase.

* Corresponding author. Tel.: +45 3075 1863; fax: +45 4466 3450.
E-mail address: MDAA@novonordisk.com (M.D. Andersen).

1387-3806/$ – see front matter © 2010 Elsevier B.V. All rights reserved.
doi:10.1016/j.ijms.2010.09.010

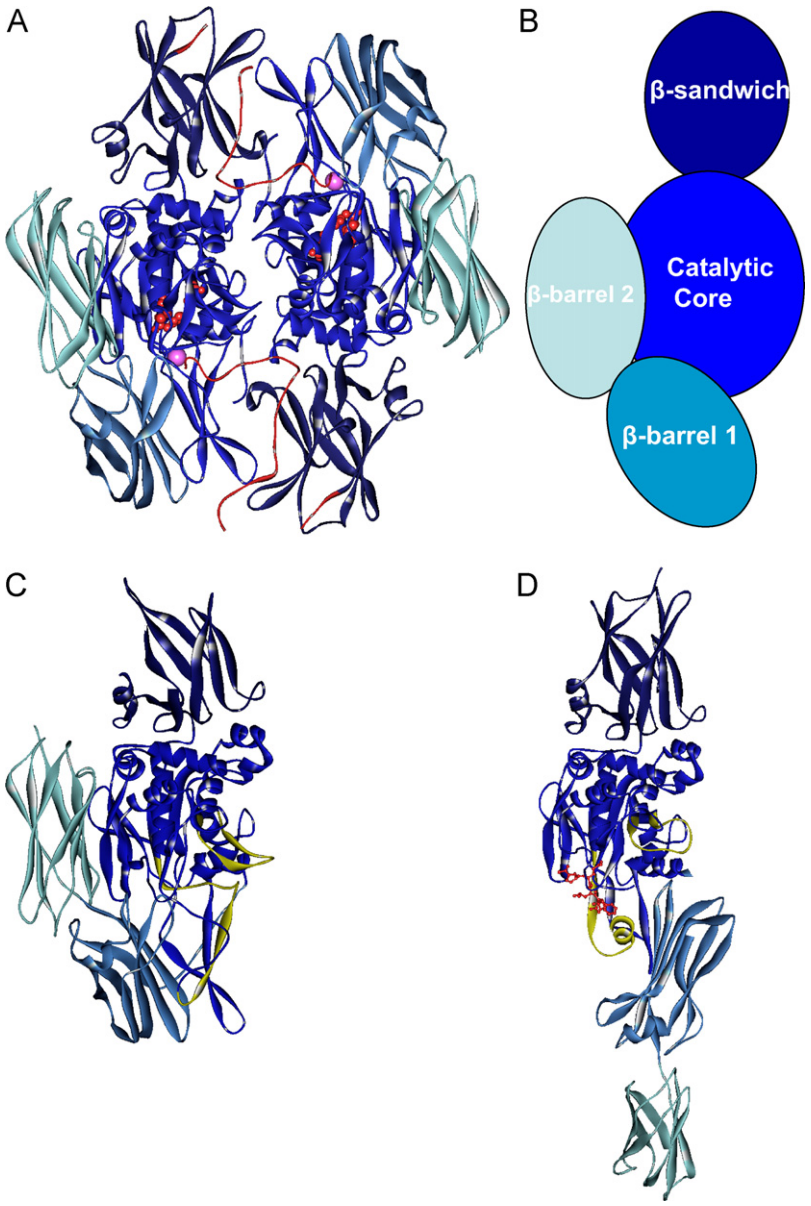

Fig. 1. rFXIII and recombinant TG2 structures and schematic domain overview. (A) The structure of rFXIII dimer. The domains are, from N- to C-terminus; activation peptide (red), β-sandwich (dark blue), catalytic core domain (blue), β-barrel 1 (light blue) and β-barrel 2 (light turquoise). The catalytic core domain contains the active site residues (Cys314, His373 and Asp396, red ball and stick) and the primary Ca^{2+} binding site (violet). (B) Schematic overview of the domain organization in rFXIII and non-activated TG2. Domain coloring is similar to panel A. (C) Non-activated TG2 and (D) activated TG2 showing the structural rearrangements in TG2 upon activation. Domain coloring is similar to panel A. Notice the reorientation of β-barrel 1 upon activation. The peptide active site inhibitor (red ball and stick) and residues 300–320 (α-helical in panel D) and 357–372 are highlighted (yellow). TG2 is monomeric and does not contain an activation peptide. The structures are from pdb-entries 1GGU, 1KV3 and 2Q3Z, respectively [10,23,26].

fibrin, FXIIIa′ undergoes a conformational change resulting in the active enzyme FXIIIa* [16–18] (Fig. 2C). During the conformational rearrangement the activation peptide and FXIII-B subunits are released. This thrombin dependent activation pathway is dominant in plasma where thrombin and fibrin is generated under coagulation conditions FXIIIa* can also be created from FXIIIa′ *in vitro* in the absence of fibrin by raising the Ca^{2+} concentration to 15 mM or higher [19]. Alternatively, zymogen FXIII is also able to activate non-proteolytic in the absence of thrombin or other proteases. Effective non-proteolytic activation of FXIII-A_2 occurs only at 50 mM Ca^{2+} and above *in vitro* [13,16]. However, even low amounts of Ca^{2+} in combination with, e.g., 1 M NaCl, chaotropic ions or other stimuli is sufficient for activation to occur [19,20]. This activation is solely an effect of a conformation change, without the release of the activation peptide, and results in rFXIIIa° (Fig. 2D). The latter activation pathway is dominant for intracellular FXIII where no thrombin is present [21,22].

FXIII belongs to a larger class of transglutaminase enzymes. The known structures of zymogen transglutaminases (FXIII, TG2 and TG3) are very similar as exemplified in Fig. 1A and C showing the structures of zymogen rFXIII and recombinant non-activated TG2, respectively [23]. Human transglutaminases are activated and regulated in numerous ways. Some transglutaminases are dependent on a proteolytic cleavage whereas others rely on conformational activation only. However, all TGs depend on Ca^{2+} for activity and activation [24]. TG2 is activated by Ca^{2+} but also inhibited by the presence of GTP/GDP nucleotide [23,25]. TG2 has been structurally characterized by X-ray crystallography in the non-active form, in the absence of nucleotides, as well as with a peptide inhibitor bound in the active site, respectively [26]. This structure of active TG2

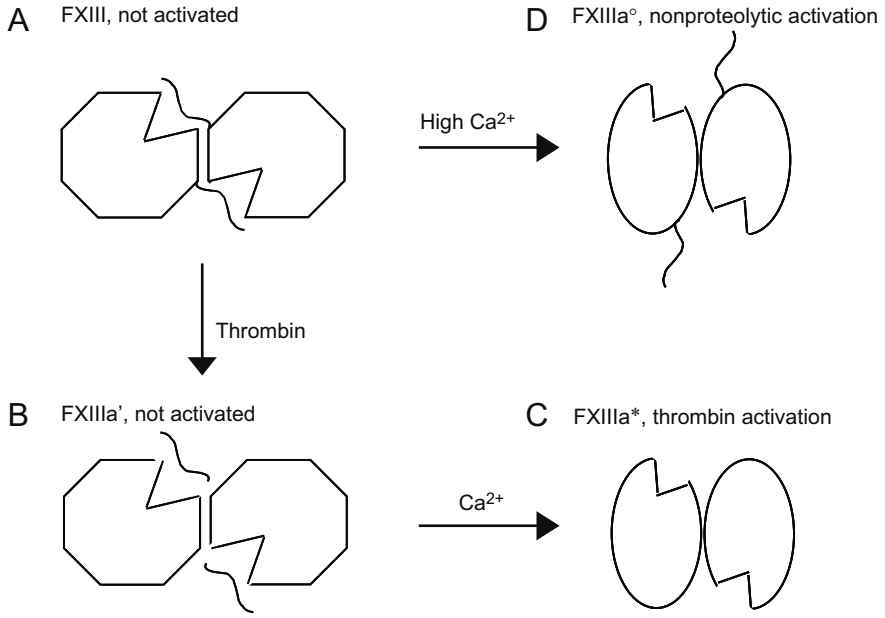

Fig. 2. Conventional view of the FXIII activation pathways. Zymogen FXIII subunit adopts a dimer structure (A) that can activate via two distinct pathways. In plasma, thrombin cleaves after residue Arg37 resulting in FXIIIa′ (B). In the presence of Ca^{2+}, FXIIIa′ can undergo a conformational change to yield the active enzyme FXIIIa* (C). Alternatively, FXIII can be activated in the presence of, e.g., 50 mM Ca^{2+} without proteolytic cleavage resulting in FXIIIa° (D).

(Fig. 1D) shows a remarkable different domain organization compared to non-activated TG2 and rFXIII. Access to the active site is created by major domain reorganizations rather than merely minor structural adjustments (Fig. 1D compared to 1A and 1C). All of the reported rFXIII crystal structures, both in the presence and absence of Ca^{2+} as well as Sr^{2+} and Yb^{2+} and even the thrombin cleaved structure in the presence of 3 mM Ca^{2+}, have been of the dimeric zymogen conformation (Fig. 1A) [10–12,15]. Little information is accessible concerning the conformation and nature of activated FXIII since it so far has eluded crystallization attempts. Thus it remains unknown whether FXIIIa° or FXIIIa* will adopt a similar domain rearrangement upon activation as found for TG2.

HX-MS has proven a powerful technique for analyzing the conformational properties of proteins in solution [27–29] and altered deuterium exchange profiles between protein states act as sensitive probes of both dynamic and structural transitions [30–36]. Furthermore, HX-MS is not confined to the conformational states of a protein that are amenable to crystallization or limited by the size of the protein, but evaluates the relevant solution state of the protein. Thus HX-MS is highly applicable for structural studies of rFXIII. The protein composes considerable 83 kDa of non-redundant sequence, i.e., 166 kDa dimer, making characterization studies highly challenging by any analytical technique available. In this study, we apply HX-MS analyses to the entire span of conformational states of rFXIII, i.e., rFXIII, rFXIIIa′, rFXIIIa* and rFXIIIa°. The deuterium exchange profiles of the rFXIII species are used to provide a rationale for the conformational changes occurring during the proteolytic and non-proteolytic activation pathways.

2. Experimental methods

2.1. rFXIII protein

Purified recombinant human FXIII expressed in *Saccharomyces cerevisiae* was obtained from Novo Nordisk A/S [37]. rFXIII is a stable dimer of the FXIII–A subunits and is equivalent to human intracellular FXIII (Fig. 1A). rFXIII was buffer exchanged and diluted to 2 mg/mL in 200 mM HEPES pH 7.4, 150 mM NaCl. This rFXIII stock was stored at 5 °C and provided the starting material for further experiments.

2.2. Preparation of rFXIIIa′, rFXIIIa*, and rFXIIIa°

- *rFXIIIa′:* rFXIII was diluted to 1 mg/mL in 200 mM HEPES pH 7.4, 150 mM NaCl. Agarose beads with thrombin covalently attached (Sigma–Aldrich Co.) was pre-equilibrated in this buffer and 100 μL beads (wet volume) was used to cleave 200 μg rFXIII in 1 h at room temperature (20 °C). Mini spin filters (Pierce Inc.) was used to entirely separate beads from protein solution. More than 95% of rFXIII was converted to rFXIIIa′ as evaluated by SDS-PAGE analysis. The resulting rFXIIIa′ was 1 mg/mL in 200 mM HEPES pH 7.4, 150 mM NaCl. rFXIIIa′ was stored at room temperature and used for experiments within 48 h.
- *rFXIIIa*:* The procedure for producing rFXIIIa′ described above was followed. However, all buffers contained an additional 50 mM $CaCl_2$. Under these conditions the thrombin activation rate of rFXIII was at least 10 fold higher than the non-proteolytic activation of rFXIII. The reaction was followed by SDS-PAGE and by generation of full enzymatic activity both in an assay using the FXIII substrate Abz-NE(CAD-DNP)EQVSPLTLLK-OH (Zedira GmbH, [38]) and in an assay measuring incorporation of monodansylcadaverine into casein [39]. The resulting rFXIIIa* was 1 mg/mL in 200 mM HEPES pH 7.4, 150 mM NaCl, 50 mM $CaCl_2$. rFXIIIa* was stored at room temperature and used for experiments within 48 h.
- *rFXIIIa°*: rFXIII was diluted to 1 mg/mL in 200 mM HEPES pH 7.4, 150 mM NaCl, 50 mM $CaCl_2$ and incubated for 1 h at 37 °C [13,16]. The reaction was followed by generation of full enzymatic activity in an assay using the FXIII substrate Abz-NE(CAD-DNP)EQVSPLTLLK-OH (Zedira GmbH, [38]) and SDS-PAGE confirmed that no proteolysis had occurred. The resulting rFXIIIa° was 1 mg/mL in 200 mM HEPES pH 7.4, 150 mM NaCl, 50 mM $CaCl_2$. rFXIIIa° was stored at room temperature and used for experiments within 48 h.

2.3. Deuterium exchange reactions

The activated forms of rFXIII have limited solubility and the protein stocks were therefore maintained at 20 °C at 1 mg/mL in 200 mM HEPES pH 7.4, 150 mM NaCl. rFXIIIa° and rFXIIIa* furthermore contained 50 mM $CaCl_2$. Zymogen rFXIII was stored at 4 °C, and diluted to 1 mg/mL and equilibrated to 20 °C before initiating exchange reactions. In-exchange of deuterium was initiated by a 10-fold dilution into 150 mM NaCl in D_2O. The final exchange reactions thus contained 0.1 mg/mL rFXIII (1.2 μM) in 20 mM HEPES pH 7.4, 150 mM NaCl, (5 mM $CaCl_2$) in final 90% D_2O. Final concentration of 5 mM $CaCl_2$ is sufficient to retain rFXIIIa° [20] and rFXIIIa* (data not shown) in the active conformation. After exchange times ranging from 10 s to 8 h at 20 °C, the reactions were quenched by adding 0.8 volumes 2 °C quench solution (Tris(2-carboxyethyl)phosphine hydrochloride, adjusted to pH 2.4 using NaOH). The quenched samples had final pH 2.5 (value measured in H_2O buffers) and contained total 100 pmol rFXIII. The samples were subjected to LC–MS analysis immediately after quenching. All sample deuterium labeling, quenching, injection to MS and timing of samples were handled by an automated set-up (Leap Technologies Inc.) as described in detail below.

2.4. Instrumentation

The HX experiments were automated by a Leap robot (H/D-x PAL; Leap Technologies Inc.) operated by the LeapShell software (Leap Technologies Inc.), which performed initiation of the deuterium exchange reaction, reaction time control, quench reaction, injection onto the UPLC system and digestion time control. The Leap robot was equipped with two temperature controlled stacks maintained at 20 °C for buffer storage, protein storage and HX reactions and maintained at 2 °C for storage of quench solution, respectively. The protein samples would in a normal HX experiment have been maintained at 2 °C, however the activated forms of rFXIII show better stability and solubility at 20 °C and this was therefore used here. The Leap robot furthermore contained a cooled Trio VS unit (Leap Technologies Inc.) holding the pepsin-, pre- and analytical columns, and the LC tubing and switching valves at 1 °C. The switching valves have been upgraded from HPLC to Microbore UHPLC switch valves (Cheminert, VICI AG). For the inline pepsin digestion, 150 μL quenched sample containing 100 pmol rFXIII was loaded and passed over a Poroszyme® Immobilized Pepsin Cartridge (2.1 mm × 30 mm (Applied Biosystems)) using a isocratic flow rate of 150 μL/min (0.1% formic acid:CH_3CN 95:5). The resulting peptides were trapped and desalted on a VanGuard pre-column BEH C18 1.7 μm (2.1 mm × 5 mm (Waters Inc.)). Subsequently, the valves were switched to place the pre-column inline with the analytical column, UPLC-BEH C18 1.7 μm (2.1 mm × 100 mm (Waters Inc.)), and the peptides separated using a 9 min gradient of 8–40% B delivered at 150 μL/min from an AQUITY UPLC system (Waters Inc.). The mobile phases consisted of A: 0.1% formic acid and B: 0.1% formic acid in CH_3CN. The ESI MS data, and the separate data dependent MS/MS acquisitions (CID) and elevated energy (MS^E) experiments were acquired in positive ion mode using a Q-Tof Premier MS (Waters Inc.). The data was obtained with a capillary voltage of 3.2 kV, cone voltage of 25 V, a MCP detector voltage of 1990 V, a desolvation gas flow of 850 L/h, a cone gas flow of 20 l/h, a desolvation temperature of 350 °C, and a source temperature of 120 °C. Leucine-enkephalin was used as the lock mass ($[M+H]^+$ ion at m/z 556.2771) and data was collected in continuum mode. During the low-energy scan of the MS^E recordings intact peptide mass spectra were obtained by maintaining collision cell energy at 10 eV, while the multiplex fragmentation MS^E spectra were obtained at ramping collision cell energies to 30 or 50 eV. Data-dependent MS/MS acquisition data was acquired using cycle of MS survey scan acquisition, and up to three subordinate targeted CID MS/MS scans.

2.5. Data analysis

Peptic peptides were identified in separate experiments using standard CID MS/MS or MS^E methods. MS^E data were processed using BiopharmaLynx 1.2 (version 017). CID data-dependent MS/MS acquisition was analyzed using the MassLynx software and in-house MASCOT database. Searches of both MS^E and data dependent CID data were conducted as non-specific digest with N-terminal acetylation of rFXIII as modification [37,40]. Results from searches against multiple sets of MS^E and CID were combined affording 90% sequence coverage of rFXIII from 79 identified peptides.

HX-MS raw data files were subjected to continuous lockmass-correction. Data analysis, i.e., centroid determination of deuterated peptides and plotting of in-exchange curves, was performed using HX-Express (Version Beta) [41]. Neither correction for H_2O content in exchange buffer nor back-exchange correction was performed since only the relative levels of deuterium incorporation of all samples were compared. The Supplementary section shows representative data for each peptide. The data generally had a standard deviations <0.2 Da, and the deviations ranged from <0.05 Da and up to 0.5 Da for some highly deuterated, low intensity peaks. Visualization of the rFXIII structure was performed using Discovery Studio Visualizer 2.5 and pdb entry 1GGU [10].

3. Results and discussion

3.1. Instrumental setup and LC–MS peptide map

HX-MS analysis with high sequence coverage of larger biomolecular systems raises the demands for efficient and reproducible separation techniques due to the increase of digest complexity. For this purpose we made use of a system setup affording automated sample preparation and sample load onto an inline hyphenation of immobilized pepsin, pre-column, UPLC C18 RP separation, and MS detection.

The inline enzymatic protein digest provided by an immobilized pepsin column generated peptides of reasonably small length (typically 10–20 amino acids). The rFXIII peptide map consisted of 79 peptic peptides identified by CID MS/MS data (44%), MS^E data (23%), or both CID MS/MS and MS^E data (33%). Fig. 3 illustrates the peptides used for HX-MS analysis mapped onto rFXIII affording 90% coverage. rFXIII contains 83 kDa of non-redundant sequence (i.e., 166 kDa dimer) and is larger than antibodies, which otherwise seems to be the largest non-redundant system analyzed by HX-MS so far [42]. However, this UPLC based setup is not at the limit of the setup and holds promise for detection and separation of even larger proteins [43]. The sequence of the first three domains of rFXIII (residues 1–628) was almost completely covered by peptic peptides. Gaps in the peptide maps represent areas where peptides were identified but the signal intensity was insufficient for proper data analysis. In contrast, the final domain (residues 629–731) seemed more stable and difficult to unfold and digest and only scattered peptides were identified in this domain.

The activated forms of rFXIII have limited stability and solubility. Therefore, the protein stocks were kept at 1 mg/ml at 20 °C. However, the signal intensity was still decreased at the later time-points and the exchange plots also display more scatter at the later time-points recorded after 8-h incubation (Supplementary material).

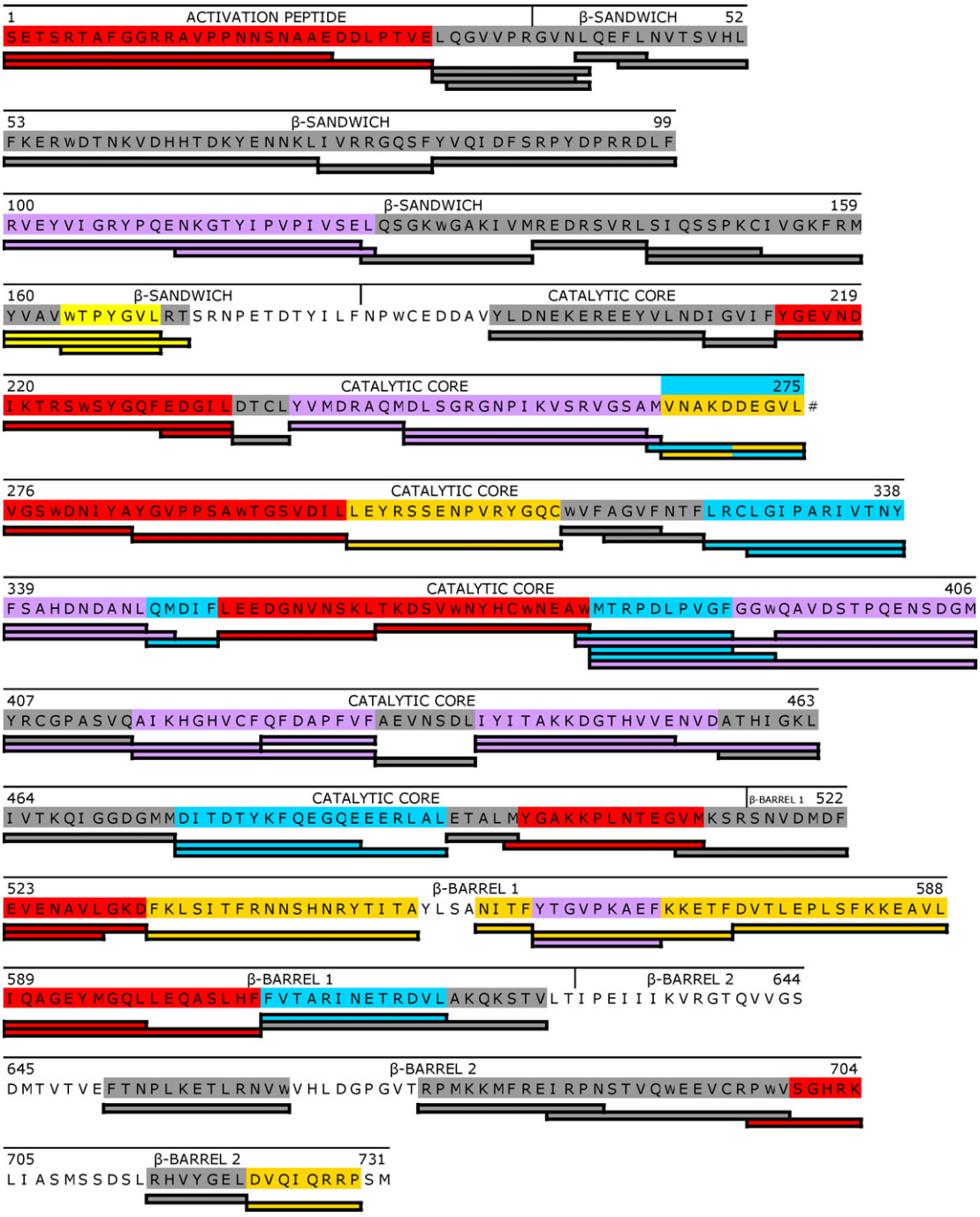

Fig. 3. Overview of rFXIII primary structure and domains showing peptides analyzed and the resulting deuterium exchange effects upon activation of rFXIII. 79 peptides covering 90% of the sequence were analyzed in up to 8 deuterium in-exchange time-points. A variety of differential effects was observed in rFXIIIa′, rFXIIIa* and rFXIIIa° relative to rFXIII: regions of rFXIII showing identical in-exchange profiles independent of activation state (grey), increased deuteration in early time-points upon activation, i.e., rFXIIIa* or rFXIIIa° (red), increased deuteration in late time-points upon activation (orange), increased deuteration upon activation as well as upon cleavage, i.e., rFXIIIa′, rFXIIIa* and rFXIIIa° (purple), decreased deuteration upon activation (blue), increased activation upon thrombin cleavage, i.e., rFXIIIa′ and rFXIIIa* (yellow). #Two distinct effects were observed in region 265–275 in the early and late timepoints, respectively.

3.2. *Changes upon thrombin cleavage of rFXIII to generate rFXIIIa′*

Thrombin cleavage in the absence of Ca^{2+} will not activate rFXIII but only produce rFXIIIa′ (Fig. 2B). rFXIIIa′ is generally assumed to have the same conformation as zymogen rFXIII, e.g., as determined in solution by the lack of solvent access to the active site Cys314 [13,14]. The majority of the rFXIIIa′ molecule does indeed display deuterium exchange curves that are equivalent to the exchange curves of zymogen rFXIII (Figs. 3 and 4A and B and Supplementary material) and this certainly suggests that the structure and domain organization of rFXIIIa′ resembles that of zymogen rFXIII. However, increased deuterium exchange was found along the entire dimer interface in rFXIIIa′ (Fig. 4A and C), as well as in a stretch (residues 560–568) in β-barrel 1 situated structurally in close proximity to the activation peptide from the opposite subunit. However, activated rFXIII species, i.e., rFXIIIa° and rFXIIIa*, display even higher exchange of deuterium in these regions (Fig. 4C and Supplementary material). Therefore rFXIIIa′ is not completely solvent exposed in these regions and the increased deuterium exchange could be a result of weakened dimer interactions upon thrombin cleavage.

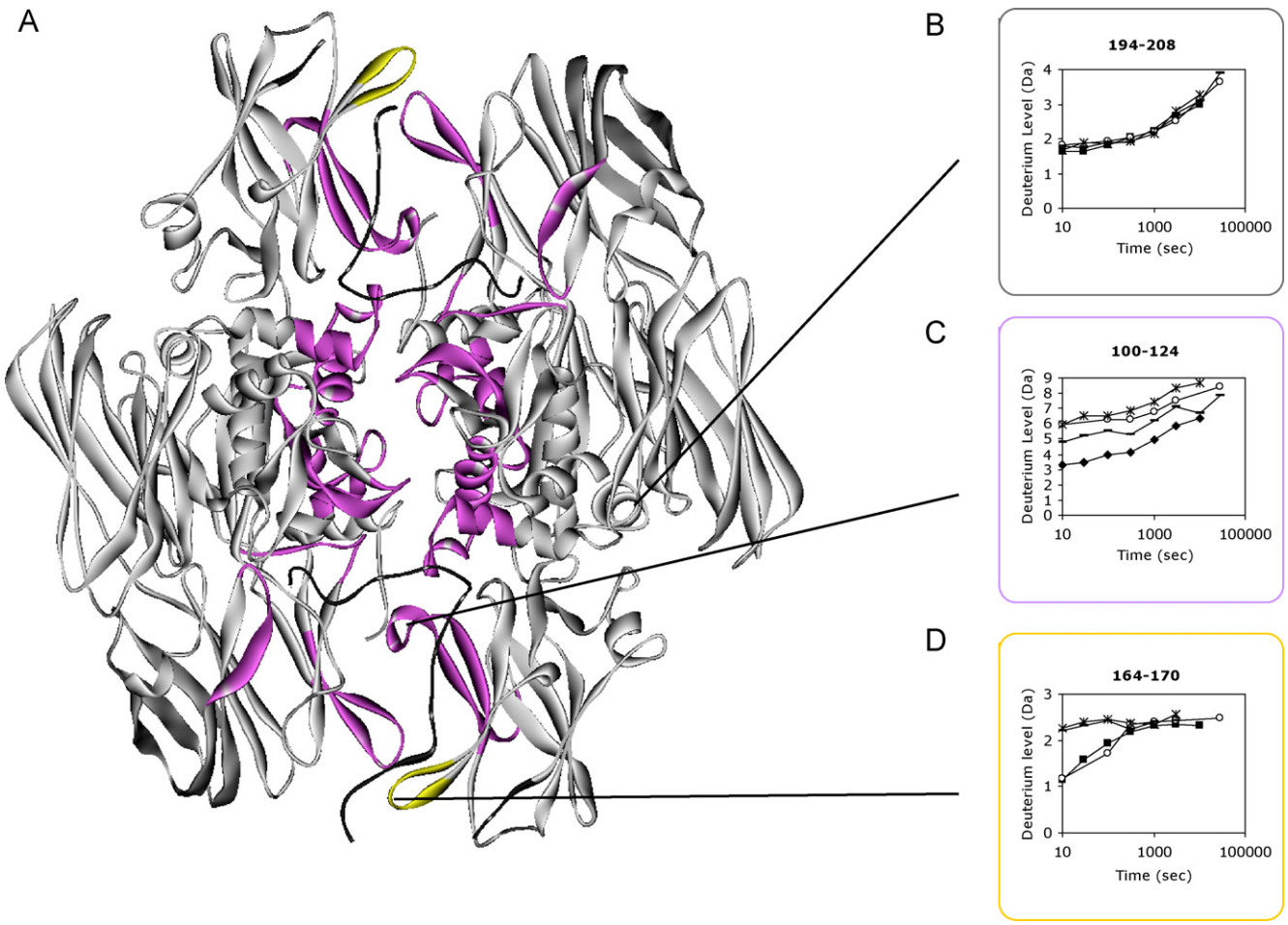

Fig. 4. Deuterium exchange effects upon thrombin cleavage of rFXIII to generate rFXIIIa′. (A) Tertiary structure of rFXIII dimer colored according to the deuterium exchange effects observed upon thrombin cleavage to generate rFXIIIa′ (color coding is similar to Fig. 3). The activation peptide is shown in black. The majority of the regions displayed identical deuterium exchange profile (grey). A large region display increased deuterium exchange in rFXIIIa′ as well as in the activated species (purple) and one region increase deuterium exchange only upon thrombin cleavage, i.e., rFXIIIa′ and rFXIIIa* (yellow). (B, C and D) Deuterium exchange plots representative for the three different patterns observed upon generation of rFXIIIa′. The deuterium exchange was followed at eight time-points ranging from 10 s up to 28,800 s (8 h) in-exchange. rFXIII species analyzed were rFXIII zymogen (■), rFXIIIa° (○), rFXIIIa′ (—) and rFXIIIa* (∗).

A small loop (residues 164–170) shows increased deuterium exchange in the cleaved forms of rFXIII, i.e., rFXIIIa′ and rFXIIIa*, but not in rFXIII or rFXIIIa° (Fig. 4A and D). Thus, this increased exchange seems to be related to thrombin cleavage, but not to activation. In accordance, this loop is positioned directly below the thrombin cleavage site (Fig. 4A, yellow) and thus becomes solvent exposed only upon thrombin cleavage but does not necessarily change stability or conformation.

3.3. Conformational changes upon complete activation to rFXIIIa*

rFXIIIa* was prepared following a similar procedure as for rFXIIIa′ but in the presence of Ca^{2+} thus causing full activation to rFXIIIa* (Fig. 2C). In contrast to zymogen rFXIII and rFXIIIa′, the active site Cys314 in rFXIIIa* is solvent accessible [13,14,44]. However, it was unknown whether major or merely minor conformational changes occur upon generation of rFXIIIa*. Using HX-MS we detect numerous changes occurring upon activation throughout the entire protein structure and 83 kDa of sequence (Figs. 3 and 5). All four domains of the molecule seem to be involved in activation but the most extensive changes are observed in the catalytic core and β-barrel 1 domains. The effects upon activation include increased deuterium exchange in early time points thus indicative of new surface being exposed (Fig. 5A and B, red) and decreased exchange in early time points thus indicative of surface region being buried (Fig. 5A and C, blue) [45,46]. Furthermore, increased deuterium exchange was also observed in some regions for late time points thus indicative of increased mobility of slow-exchanging regions, e.g., regions that are bound in secondary structure or regions buried in the protein structure (Fig. 5A and D, orange) [45,46].

- *the dimer interface:* Similar to rFXIIIa′, the entire dimer interface of rFXIIIa* displays increased deuterium exchange for the early time points (Fig. 5A and B) thus new residues are becoming solvent exposed. This indicates dramatic effects on the rFXIII dimer structure upon activation and suggests that either rFXIIIa* is monomeric similar to TG2 or that the dimer interactions have been weakened even further compared to rFXIIIa′ and extensively weakened compared to zymogen rFXIII.
- *β-sandwich domain:* The N-terminal β-sandwich domain is largely unaffected upon activation to rFXIIIa* and the only effect observed is increased solvent exposure of the dimer interface.
- *Catalytic core domain*: In contrast, widespread effects are observed in the catalytic core domain involving both exposure and burial of surface as well as increased structural dynamics (Figs. 3 and 6). Although HX-MS data does not reveal conformational changes at neither atomic nor residue level it is apparent that “the front face” of the molecule (Fig. 6, left panel) becomes more dynamic and exposes more surface upon activation. This

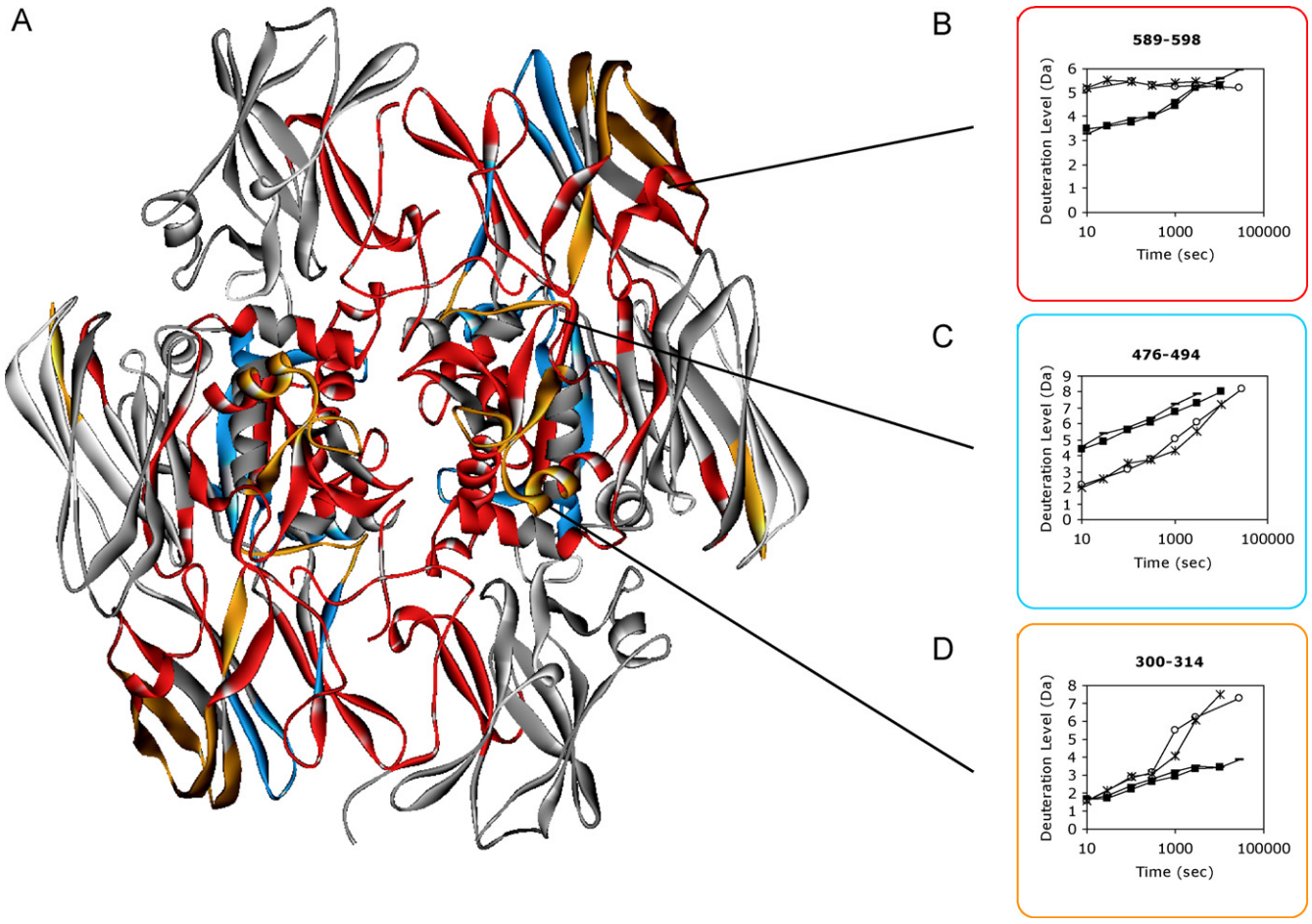

Fig. 5. Deuterium exchange effects upon activation of rFXIII to generate rFXIIIa*. (A) Tertiary structure of rFXIII dimer showing the regions displaying identical deuterium exchange profile upon activation to generate rFXIIIa* (grey). Colored regions indicate changed deuterium exchange in rFXIIIa* relative to rFXIII: increased deuteration upon activation in the early timepoints (red), increased deuteration upon activation in late timepoints (orange) and decreased deuteration upon activation (blue). (B, C and D) Deuterium exchange plots representative for the three different patterns observed upon generation of rFXIIIa*. The deuterium exchange was followed at eight time-points ranging from 10 s up to 28,800 s (8 h) in-exchange. rFXIII species analyzed were rFXIII zymogen (■), rFXIIIa◦ (○), rFXIIIa′ (—) and rFXIIIa* (∗).

"front face" of the molecule holds the entry to the active site and increased dynamic changes may create the necessary access to the active site and in particular to the catalytic Cys314. In contrast, effects relating to structural surface burial are observed for the opposite "back face" of the molecule (Fig. 6, right panel). The extensive deuterium exchange effects on the catalytic core domain of rFXIIIa* can be explained in the context of the structural domain reorganizations taking place in TG2 upon activation

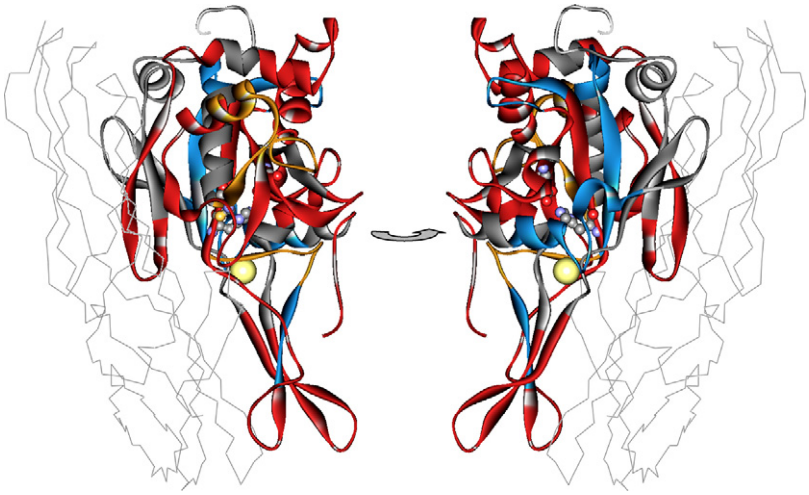

Fig. 6. The activation effects on the catalytic core domain. The catalytic core domain is shown in ribbon and colored according to Fig. 5. β-barrels 1 and 2 are shown in grey Cα wire. Active site residues Cys314, His373 and Asp396 (ball and stick) and Ca^{2+} (yellow sphere) are shown. Left panel is oriented similar to the left subunit of the dimer in other figures and shows the "front face" of the molecule. The right panel has been rotated 180◦ to show the opposite "back face" of the molecule.

(Fig. 1C and D). The catalytic core domain of TG2 seems predominantly structurally unaltered upon activation. However, two segments change dramatically (Fig. 1C and D, both segments depicted in yellow). Upon activation, a segment rearranges from β-strand (Fig. 1C) to α-helix (Fig. 1D, TG2 residues 300–320, yellow) and a loop positioned in close structural proximity above (Fig. 1C, TG2 residues 357–372, yellow) changes conformation and seems to adapt less secondary structure upon activation (Fig. 1D). The result of these rearrangements in the catalytic core domain of TG2 is most notably that the TG2 β-barrel 1 changes orientation and is shifted away from the entry to the active site (Fig. 1D, active site inhibitor shown in red). The data obtained for rFXIIIa* relative to zymogen rFXIII are in accordance with these observations made for TG2 upon activation as described in further detail below. Notably, residues 349–353 in rFXIIIa* (Fig. 6, lower blue β-strand), which corresponds structurally to TG2 residues 310–320 changing from β-strand to α-helix upon activation (Fig. 1D, yellow helix), shows decreased deuterium exchange upon activation of rFXIII to rFXIIIa* (Figs. 3 and 6). Decreased exchange may be expected from a β-strand at the edge of a β-sheet, with only half of the backbone amide proteins engaged in hydrogen bonding, when rearranging to an α-helix, where all backbone amide protons form hydrogen bonds. Similarly, residues 400–406 in rFXIIIa* corresponding structurally to the TG2 loop changing conformation upon activation (Fig. 1C and D, residues 357–372, depicted in yellow) show increased deuterium exchange in rFXIIIa* (Figs. 3 and 6). However, the effects of increased solvent access in the dimer interface cannot be distinguished from the effects of a potential structural difference in this loop.

- *β-barrel 1:* The HX-MS data of rFXIIIa* also reflects a possible reorientation of β-barrel 1 as observed in TG2 upon activation (Fig. 1C and D). Residues 607–619 of rFXIII β-barrel 1 shows decreased deuterium exchange in the early time points upon activation, thus indicative of surface region being buried (Figs. 3 and 5A, blue segment in β-barrel 1). The structurally corresponding segment in TG2 is fully solvent exposed in non-activated TG2 (Fig. 1C) whereas it packs against the catalytic core domain in activated TG2 (Fig. 1D) consistent with decreased deuterium exchange. Furthermore, this β-barrel 1 segment in activated TG2 seems to create new interactions with an α-helix in the catalytic core domain of TG2. Correspondingly, the same α-helix in rFXIIIa* (residues 476–494) shows substantially decreased deuterium exchange relative to rFXIII (Figs. 3 and 6, central blue helix in right panel). In contrast, the opposite end of rFXIIIa* β-barrel 1 which is facing β-barrel 2 (residues 523–532, 560–568 and 589–606) (Fig. 5B) should change from packing closely to both β-barrel 2 and the catalytic core domain in the inactive structure (Figs. 1A and 5A) to only a loose association with β-barrel 2 in the possible extended activated structure (Fig. 1D). Such a reorientation would result in increased solvent exposure in this end of β-barrel 1 and in accordance these regions do indeed display increased deuterium exchange (Figs. 3 and 5A and B).
- *β-barrel 2:* Unfortunately, rFXIII β-barrel 2 was rather difficult to digest and lower sequence coverage was obtained (Fig. 3). Most of the segments analyzed did not display any changes upon activation (Figs. 3 and 5A). One of the rFXIII β-barrel 2 loops (residues 697–704) which is packed against the catalytic core domain in zymogen rFXIII, did nevertheless display increased deuteration upon activation consistent with the full surface exposed orientation seen in the corresponding segment in TG2 (Figs. 1D, 3 and 5A). Furthermore, both β-barrels 1 and 2 in rFXIII have regions of increased dynamics (Figs. 3 and 5A, orange) consistent with the elongated activated structure of TG2 being less tightly packed.

Finally, it is important to note that although the HX-MS data for all of the domains of rFXIII are in accordance with the structural reorganizations observed in TG2 upon activation; this does not actually prove that the same rearrangements take place in rFXIII. However, the HX-MS data supports that they could occur and given the striking structural similarity of rFXIII and TG2 it is possible that the same conformational re-arrangements could take place in rFXIIIa* and activated TG2.

3.4. *rFXIIIa* and rFXIIIa◦ are conformationally indistinguishable*

Whereas rFXIIIa* is prepared by thrombin cleavage at 20 °C in the presence of Ca^{2+}, rFXIIIa◦ is simply prepared by incubation of rFXIII at 37 °C in 50 mM Ca^{2+} without proteolytic cleavage. Full activation of rFXIIIa* and rFXIIIa◦ was confirmed by enzymatic activity assays (data not shown). Aside from the N-terminal activation peptide region, absent in rFXIIIa*, all the deuterium exchange profiles are similar for rFXIIIa* and rFXIIIa◦ (Figs. 3, 5 and 6 and Supplementary material). Therefore, all the conformational and dynamic changes that takes place in rFXIIIa* also occurs in rFXIIIa◦. The HX-MS data very clearly demonstrate that both the thrombin dependent and the non-proteolytic activation pathways of rFXIII (Fig. 2) produce structurally similar active forms of rFXIII.

The primary structure of rFXIIIa* and rFXIIIa◦ differs only by lack of the first 37 residues (the activation peptide) in rFXIIIa*. HX-MS data indicate that this region is highly solvent exposed in both zymogen rFXIII and rFXIIIa◦. However, a slightly lower exchange observed in rFXIII relative to rFXIIIa◦ indicates that the activation peptide adopts a different and more solvent exposed conformation in rFXIIIa◦ (Supplementary material). The activation peptide region should be free in solution after thrombin cleavage and full activation to rFXIIIa* [47] and thus fully solvent exposed. For reference, deuterium exchange of region 1–30 in rFXIIIa′ and rFXIIIa* were therefore analyzed. The exchange pattern in region 1–30 in rFXIIIa′, rFXIIIa* and rFXIIIa◦ is identical suggesting full solvent exposure of 1–30 in rFXIIIa◦ (Supplementary material). The HX-MS data suggest a difference between the activation peptide of rFXIIIa◦ and zymogen rFXIII only up to residue 30, after this position the exchange profiles are similar. Furthermore, rFXIIIa◦ does not display increased deuterium exchange in segment 164–170 structurally positioned directly below the thrombin cleavage site at residue 37 (see Section 3.2 and Fig. 4A and D). Therefore, the activation peptide appears to changes conformation in rFXIIIa◦ only in the region up to residue 30.

It has previously been proposed that some regions in assumed rFXIIIa* and rFXIIIa◦ species have structural differences [48–50]. These studies were performed using chemical modification techniques or MALDI-MS detected HX with 29% sequence coverage [48–50]. Furthermore, these studies were done under conditions where activated rFXIII, in our hands, is not stable and deactivates due to insufficient Ca^{2+} levels, i.e., 0–1 mM $CaCl_2$ (Kristiansen and Andersen, data not shown). This underscores both the responsive nature of the various activation states of rFXIII species as well as the need to keep strict control of FXIII catalytic activity and Ca^{2+} levels particularly in the final deuterium exchange buffer.

4. Conclusions

rFXIII has been analyzed by HX-MS in several conformational states, rFXIII, rFXIIIa′, rFXIIIa* and rFXIIIa◦. The activated forms of rFXIII have so far eluded crystallization attempts and the 83 kDa size of rFXIII is out of the range for NMR. Although HX-MS can never reveal actual protein structures and cannot reveal the struc-

ture of the activated forms of rFXIII, the technology as used here has offered clear suggestions to the conformational changes occurring upon activation of rFXIII. The HX-MS data show increased deuterium exchange along the entire dimer interface suggesting weakened dimer interaction in both rFXIIIa′, rFXIIIa* and rFXIIIa°. Aside from this, rFXIIIa′ resembles zymogen rFXIII and no conformational changes seem to have taken place. In contrast, extensive changes occur upon full activation of rFXIII to either rFXIIIa* or rFXIIIa°. The changes in the active molecules occur primarily in the catalytic core and β-barrel 1 domains and are in accordance with the changes observed in TG2 upon activation. While these data do not provide strict evidence that the same conformational changes are actually occurring in TG2 and rFXIII upon activation, they do offer a plausible explanation for the HX-MS data obtained with rFXIII. Furthermore, our experiments show highly similar HX-MS data for rFXIIIa* and rFXIIIa° clearly demonstrating that both the thrombin dependent and the non-proteolytic activation pathways of rFXIII produce similar activated conformations of the molecules.

Acknowledgements

The authors wish to thank Betina Ørtberg Olsen and Brian Rosenberg for excellent technical assistance, Drs. Lene Hørlyck and Eva H.N. Olsen for critical reading of the manuscript and Peter D. Smith, Leap Technologies Inc. for excellent support in customizing the Leap Robotics platform and LeapShell software for our use.

Appendix A. Supplementary data

Supplementary data associated with this article can be found, in the online version, at doi:10.1016/j.ijms.2010.09.010.

References

[1] L. Muszbek, R.A. Ariens, A. Ichinose, Factor XIII: recommended terms and abbreviations, J. Thromb. Haemost. 5 (2007) 181–183.
[2] G.M. Asijee, L. Muszbek, J. Kappelmayer, J. Polgár, A. Horváth, A. Sturk, Platelet vinculin: a substrate of activated factor XIII, Biochim. Biophys. Acta 954 (1988) 303–308.
[3] K. Serrano, D.V. Devine, Intracellular factor XIII crosslinks platelet cytoskeletal elements upon platelet activation, Thromb. Haemost. 88 (2002) 315–320.
[4] A. Jayo, I. Conde, P. Lastres, V. Jiménez-Yuste, C. González-Manchón, New insights into the expression and role of platelet factor XIII-A, J. Thromb. Haemost. 7 (2009) 1184–1191.
[5] R.A. Ariëns, T.S. Lai, J.W. Weisel, C.S. Greenberg, P.J. Grant, Role of factor XIII in fibrin clot formation and effects of genetic polymorphisms, Blood 100 (2002) 743–754.
[6] L. Lorand, Factor XIII: structure, activation, and interactions with fibrinogen and fibrin, Ann, N. Y. Acad. Sci. 936 (2001) 291–311.
[7] L. Muszbek, V.C. Yee, Z. Hevessy, Blood coagulation factor XIII: structure and function, Thromb. Res. 94 (1999) 271–305.
[8] M. Karimi, Z. Bereczky, N. Cohan, L. Muszbek, Factor XIII deficiency, Semin. Thromb. Hemost. 35 (2009) 426–438.
[9] A. Ichinose, Extracellular transglutaminase: factor XIII, Transglutaminases: Family Enzymes Diverse Funct. 38 (2005) 192–208.
[10] B.A. Fox, V.C. Yee, L.C. Pedersen, I.L. Trong, P.D. Bishop, R.E. Stenkamp, D.C. Teller, Identification of the calcium binding site and a novel ytterbium site in blood coagulation factor XIII by X-ray crystallography, J. Biol. Chem. 274 (1999) 4917–4923.
[11] M.S. Weiss, H.J. Metzner, R. Hilgenfeld, Two non-proline cis peptide bonds may be important for factor XIII function, FEBS Lett. 423 (1998) 291–296.
[12] V.C. Yee, L.C. Pedersen, I. Le-Trong, P.D. Bishop, R.E. Stenkamp, D.C. Teller, Three-dimensional structure of a transglutaminase: human blood coagulation factor XIII, Proc. Natl. Acad. Sci. U. S. A. 91 (1994) 7296–7300.
[13] R.B. Credo, C.G. Curtis, L. Lorand, Ca2+-related regulatory function of fibrinogen, Proc. Natl. Acad. Sci. U. S. A. 75 (1978) 4234–4237.
[14] C.G. Curtis, K.L. Brown, R.B. Credo, R.A. Domanik, A. Gray, P. Stenberg, L. Lorand, Calcium-dependent unmasking of active center cysteine during activation of fibrin stabilizing factor, Biochemistry 13 (1974) 3774–3780.
[15] V.C. Yee, L.C. Pedersen, P.D. Bishop, R.E. Stenkamp, D.C. Teller, Structural evidence that the activation peptide is not released upon thrombin cleavage of factor XIII, Thromb. Res. 78 (1995) 389–397.
[16] T.J. Hornyak, J.A. Shafer, Interactions of factor XIII with fibrin as substrate and cofactor, Biochemistry 31 (1992) 423–429.
[17] T.J. Janus, S.D. Lewis, L. Lorand, J.A. Shafer, Promotion of thrombin-catalyzed activation of factor XIII by fibrinogen, Biochemistry 22 (1983) 6269–6272.
[18] C.S. Greenberg, K.E. Achyuthan, J.W.d. Fenton, Factor XIIIa formation promoted by complexing of alpha-thrombin, fibrin, and plasma factor XIII, Blood 69 (1987) 867–871.
[19] L Lorand, R.B. Credo, T.J. Janus, Factor XIII (fibrin-stabilizing factor), Methods Enzymol. 80 (1981) 333–341.
[20] J. Polgár, V. Hidasi, L. Muszbek, Non-proteolytic activation of cellular protransglutaminase (placenta macrophage factor XIII), Biochem. J. 267 (1990) 557–560.
[21] L. Muszbek, G. Haramura, J. Polgar, Transformation of cellular factor-XIII into an active zymogen transglutaminase in thrombin-stimulated platelets, Thromb. Haemost. 73 (1995) 702–705.
[22] L. Muszbek, J. Polgar, Z. Boda, Platelet factor-XIII becomes active without the release of activation peptide during platelet activation, Thromb. Haemost. 69 (1993) 282–285.
[23] S. Liu, R.A. Cerione, J. Clardy, Structural basis for the guanine nucleotide-binding activity of tissue transglutaminase and its regulation of transamidation activity, Proc. Natl. Acad. Sci. U. S. A. 99 (2002) 2743–2747.
[24] L. Lorand, R.M. Graham, Transglutaminases: crosslinking enzymes with pleiotropic functions, Nat. Rev. Mol. Cell Biol. 4 (2003) 140–156.
[25] G.E. Begg, L. Carrington, P.H. Stokes, J.M. Matthews, M.A. Wouters, A. Husain, L. Lorand, S.E. Iismaa, R.M. Graham, Mechanism of allosteric regulation of transglutaminase 2 by GTP, Proc. Natl. Acad. Sci. U. S. A. 103 (2006) 19683–19688.
[26] D.M. Pinkas, P. Strop, A.T. Brunger, C. Khosla, Transglutaminase 2 undergoes a large conformational change upon activation, PLoS Biol. 5 (2007) e327.
[27] A. Hvidt, K. Linderstrøm-Lang, Exchange of hydrogen atoms in insulin with deuterium atoms in aqueous solutions, Biochim. Biophys. Acta 14 (1954) 574–575.
[28] Z. Zhang, D.L. Smith, Determination of amide hydrogen exchange by mass spectrometry: a new tool for protein structure elucidation, Protein Sci. 2 (1993) 522–531.
[29] A. Hvidt, S.O. Nielsen, Hydrogen exchange in proteins, in: Adv. Protein Chem., Academic Press, 1966, pp. 287–386.
[30] K.D. Rand, T.J.D. Jørgensen, O.H. Olsen, E. Persson, O.N. Jensen, H.R. Stennicke, M.D. Andersen, Allosteric activation of coagulation factor VIIa visualized by hydrogen exchange, J. Biol. Chem. 281 (2006) 23018–23024.
[31] T.E. Wales, J.R. Engen, Hydrogen exchange mass spectrometry for the analysis of protein dynamics, Mass Spectrom. Rev. 25 (2006) 158–170.
[32] J.J. Englander, C. Del Mar, W. Li, S.W. Englander, J.S. Kim, D.D. Stranz, Y. Hamuro, V.L. Woods, Protein structure change studied by hydrogen–deuterium exchange, functional labeling, and mass spectrometry, Proc. Natl. Acad. Sci. U. S. A. 100 (2003) 7057–7062.
[33] C.H. Croy, J.R. Koeppe, S. Bergqvist, E.A. Komives, Allosteric changes in solvent accessibility observed in thrombin upon active site occupation, Biochemistry 43 (2004) 5246–5255.
[34] K.L. Hailey, S. Li, M.D. Andersen, M. Roy, V.L. Woods, P.A. Jennings, Pro-interleukin (IL)-1β shares a core region of stability as compared with mature IL-1β while maintaining a distinctly different configurational landscape, J. Biol. Chem. 284 (2009) 26137–26148.
[35] A.N. Hoofnagle, K.A. Resing, N.G. Ahn, Protein analysis by hydrogen exchange mass spectrometry, Annu. Rev. Biophys. Biomol. Struct. 32 (2003) 1–25.
[36] S.W. Englander, M.M.G. Krishna, Hydrogen exchange, Nat. Struct. Mol. Biol. 8 (2001) 741–742.
[37] P.D. Bishop, D.C. Teller, R.A. Smith, G.W. Lasser, T. Gilbert, R.L. Seale, Expression, purification, and characterization of human factor XIII in *Saccharomyces cerevisiae*, Biochemistry 29 (1990) 1861–1869.
[38] K Oertel, A. Hunfeld, E. Specker, C. Reiff, R. Seitz, R. Pasternack, J. Dodt, A highly sensitive fluorometric assay for determination of human coagulation factor XIII in plasma, Anal. Biochem. 367 (2007) 152–158.
[39] L. Lorand, T. Urayama, J.W.C. de Kiewiet, H.L. Nossel, Diagnostic and genetic studies on fibrin-stabilizing factor with a new assay based on amine incorporation, J. Clin. Invest. 48 (1969) 1054–1064.
[40] N. Takahashi, Y. Takahashi, F.W. Putnam, Primary structure of blood coagulation factor XIIIa (fibrinoligase, transglutaminase) from human placenta, Proc. Natl. Acad. Sci. U. S. A. 83 (1986) 8019–8023.
[41] D.D. Weis, J.R. Engen, I.J. Kass, Semi-automated data processing of hydrogen exchange mass spectra using HX-express, J. Am. Soc. Mass Spectrom. 17 (2006) 1700–1703.
[42] D. Houde, J. Arndt, W. Domeier, S. Berkowitz, J.R. Engen, Characterization of IgG1 conformation and conformational dynamics by hydrogen/deuterium exchange mass spectrometry, Anal. Chem. 81 (2009) 5966.
[43] T.E. Wales, K.E. Fadgen, G.C. Gerhardt, J.R. Engen, High-speed and high-resolution UPLC separation at zero degrees celsius, Anal. Chem. 80 (2008) 6815–6820.
[44] T.J. Hornyak, J.A. Shafer, Role of calcium ion in the generation of factor XIII activity, Biochemistry 30 (1991) 6175–6182.
[45] R.A. Garcia, D. Pantazatos, F.J. Villarreal, Hydrogen/deuterium exchange mass spectrometry for investigating protein–ligand interactions, ASSAY Drug Dev. Technol. 2 (2004) 81–91.
[46] J.G. Mandell, A.M. Falick, E.A. Komives, Identification of protein–protein interfaces by decreased amide proton solvent accessibility, Proc. Natl. Acad. Sci. U. S. A. 95 (1998) 14705–14710.

[47] E. Ortner, V. Schroeder, R. Walser, O. Zerbe, H.P. Kohler, Sensitive and selective detection of free FXIII activation peptide: a potential marker of acute thrombotic events, Blood 115 (2010) 5089–5096.
[48] T.M. Sabo, P.B. Brasher, M.C. Maurer, Perturbations in factor XIII resulting from activation and inhibition examined by solution based methods and detected by MALDI-TOF MS, Biochemistry 46 (2007) 10089–10101.
[49] B.T. Turner, M.C. Maurer, Evaluating the roles of thrombin and calcium in the activation of coagulation factor XIII using H/D exchange and MALDI-TOF MS, Biochemistry 41 (2002) 7947–7954.
[50] B.T. Turner, T.M. Sabo, D. Wilding, M.C. Maurer, Mapping of factor XIII solvent accessibility as a function of activation state using chemical modification methods, Biochemistry 43 (2004) 9755–9765.